Journal of Materials Chemistry

Cite this: J. Mater. Chem., 2012, 22, 24463

www.rsc.org/materials

PAPER

Reducing recombination in ZnO photoanodes for dye sensitised solar cells through simple chemical synthesis

Lioz Etgar,†*[ad] James S. Bendall,†[b] Vincent Laporte,[c] Mark E. Welland[b] and Michael Graetzel[a]

Received 24th July 2012, Accepted 6th September 2012
DOI: 10.1039/c2jm34904c

A method has been developed to synthesise zinc oxide nanowire arrays that demonstrate superior device performance compared to conventional ZnO nanowires within dye sensitised solar cells (DSSCs). This simple yet effective methodology has produced nanowires with triple device performance when compared to conventional ZnO nanowire DSSCs. We have fully characterised the morphology and physical properties of these wires and have demonstrated that the device improvements are due to a reduction in the recombination centres associated with the ZnO crystal.

Introduction

The dye-sensitised solar cell (DSSC) is a promising photovoltaic device, currently receiving enormous attention from research groups worldwide.[1] It differs widely from conventional silicon-based solar cells, not only in the way charges are separated and transported but also in its design and construction. Its low-cost, lightweight architecture affords much greater flexibility in terms of integration into emerging technologies and it offers much promise in the field of sustainable energy solutions.

Traditionally, DSSCs have been constructed using highly porous, high surface-to-volume ratio TiO_2 nanoparticle films that allow high concentrations of dye loading and relatively high photon–electron conversion efficiency.[2] Other materials have been suggested as alternative candidates for photoanodes – zinc oxide, tin oxide and copper oxide to name just a few. Zinc oxide is emerging as one of the most promising materials[3] with a band gap almost identical to that of TiO_2 (~3.3 eV) yet with faster electron mobility; it has been predicted to be a superior material than TiO_2, electronically at least. Several studies have shown promising power conversion efficiency when using ZnO nanoparticles.[4,5] Additionally, it has the ability to be grown easily in various morphologies such as wires, nanoparticles and hierarchical nanostructures, which opens up the possibility for tailoring the films' structure and physico-chemical properties.[6] Moreover with many of the growth procedures taking place under aqueous conditions some level of chemical control is possible leading to, for example, dopant incorporation.[7]

A DSSC works on the principle that an excited electron can travel through the porous metal oxide scaffold before finding its way to the external circuitry. In TiO_2 nanoparticle films some electron hopping must occur across the nanoparticle–nanoparticle grain boundaries, which can often lead to loss of cell performance and recombination with the excited sensitizer or the electrolyte. It has been suggested that nanowires may offer an improved route for electron transport; fewer grain boundaries should ensure faster electron kinetics. Zinc oxide, easily grown into nanowire structures, should be an ideal material for the DSSC.[8] Nevertheless, ZnO-based devices still seriously lag behind TiO_2 devices for a number of reasons, mainly due to unstable surface traps on the ZnO crystal that induce facile electron–hole recombination to occur. Various methodologies exist to try and circumvent this problem, including the use of core–shell structures such as titania- or magnesia-coated ZnO nanowires.[9] The purpose of the shells is to quench the surface-related defects and therefore the recombination centres on the wire.[10]

In this paper we describe a simple yet effective method to produce a highly stable and crystalline ZnO NW film that has lower recombination centres, without the necessity for an additional shell. These wires show extremely promising performance within DSSCs. We achieve this by adding a rare earth additive into the growth solution, and we have fully characterised the structure and properties of the resultant films.

Experimental

Nanowire growth and characterisation

Substrates were initially cleaned in acetone, isopropanol and deionised water and dried under nitrogen. Substrates used were either FTO-coated glass (Solaronix FTO22-15) or silicon wafer coated with a native oxide layer. Thin layers of the zinc metal

[a]*Laboratory for Photonics and Interfaces, Swiss Federal Institute of Technology, CH 1015, Lausanne, Switzerland. E-mail: lioz.etgar@epfl.ch, lioz.etgar@mail.huji.ac.il*
[b]*Nanoscience Centre, University of Cambridge, 11 JJ Thomson Ave, Cambridge, CB3 0FF, UK*
[c]*Interdisciplinary Centre for Electron Microscopy, Swiss Federal Institute of Technology, CH 1015, Lausanne, Switzerland*
[d]*Institute of Chemistry, The Hebrew University, Jerusalem 91904, Israel*
† Both authors contributed equally to this work.

were sputtered onto the substrates (Emitech K575x sputter coater system) at 100 mA through a shadow mask (6 mm^2) in order to define the active area. Seeded substrates were placed into a growth solution at 92 °C. Reactant species, concentrations and growth times are outlined in Table 1. After the specified growth time, substrates were removed, cleaned in deionised water and dried. Zinc nitrate hydrate (Sigma-Aldrich 99.999%), yttrium nitrate (Sigma-Aldrich 99.8%), polyethylenimine (Sigma-Aldrich end-capped average $M_w \sim 800$ by LS, average $M_n \sim 600$ by GPC) and hexamethylene tetramine (Alfa Aesar 99+%) were used as supplied.

SEM and EDX characterisation was carried out on a Carl Zeiss FEG-SEM (Leo Gemini Column) operated at 10 keV with an Inlens detector and an integrated EDX detector (Oxford Instruments). For TEM characterisation, specimens were imaged using a JEOL 4000EX microscope operating at 400 kV and an FEI Tecnai F20 microscope operating at 200 kV.

XRD was carried out using a Bruker D8 diffractometer in reflection mode. Raman spectroscopy was performed on a Renishaw spectrometer through a 50× objective and in the backscattering geometry. A He–Ne laser at 632.8 nm (1.96 eV) was used for excitation. The nanowire film was grown on a silicon substrate under identical conditions to the FTO–glass nanowires. Photoluminescence spectroscopy was acquired with an excitation wavelength of 325 nm.

X-ray Photoelectron Spectroscopy (XPS) data were collected by an Axis Ultra instrument (Kratos analytical, Manchester, UK) under ultra-high vacuum conditions (<10–8 Torr) and using a monochromatic Al Kα X-ray source (1486.6 eV) in the Surface Analysis Facility of the Interdisciplinary Centre for Electron Microscopy at EPFL.

The source power was maintained at 150 W and the emitted photoelectrons were sampled from an Ø 200 μm area.

The photoelectron take-off angle, between the surface and the direction in which the photoelectrons were analyzed, was 90°. The analyzer pass energy was 80 eV for survey spectra and 40 eV for high-resolution spectra. The adventitious carbon 1s peak was calibrated at 285 eV and used as an internal standard to compensate for any charging effects. Sputtering of the surface by a 3 keV Argon ion beam was used to depth profile the samples with an estimated crater size of 1 × 1 mm^2. The etch rate was approximately 4 nm min^{-1}. Both curve fitting of the spectra and quantification were performed with the CasaXPS software, using relative sensitivity factors given by Kratos.

Table 1 Growth conditions for the ZnO samples used in this study

Sample name	$[Zn(NO_3)_2]$ (M)	[HMT] (M)	$[Y(NO_3)_3]$ (M)	[PEI] (M)	Growth time (h)
ZnO	0.07	0.05	—	—	2
ZnO-a	0.07	0.05	0.0035	—	2
ZnO-b	0.07	0.05	0.007	—	2
ZnO-c	0.07	0.05	0.014	—	2
ZnO-d	0.07	0.05	0.014	0.007	24
ZnO-e	0.07	0.05	0.014	0.007	6–20[a]

[a] Depending on the length required. Growth took place in alternate solutions, swapping every 2 hours. Solutions were: (1) $Zn(NO_3)_2$, HMT, $Y(NO_3)_3$; (2) $Zn(NO_3)_2$, HMT, PEI.

Solar cell fabrication

The ZnO NW film was stained by immersing it into a dye solution of C220 in a mixture of acetonitrile and *tert*-butanol (volume ratio 1 : 1) for 4 hours.[11] The dye-sensitized solar cell was assembled by sandwiching the dye-sensitized ZnO-NWs semiconductor component with the Pt-coated FTO cathode using a piece of hot melt Surlyn (25 μm thick) as a spacer. The internal space was filled with a redox electrolyte consisting of 1.0 M DMII, 50 mM LiI, 30 mM I_2, 0.5 M TBP, and 0.1 M GNCS in a mixture of acetonitrile and valeronitrile (V/V, 85/15).

Photovoltaic characterisation

For photovoltaic measurements we employed an AM 1.5 solar simulator equipped with a 450 W xenon lamp (Model no. 81172, Oriel). Its output was calibrated to 100 MW cm^{-2} by using a reference Si photodiode equipped with an IR-cutoff filter (KG-3, Schott) in order to reduce the mismatch between the simulated light and AM 1.5 (in the region of 350–750 nm) to less than 2% with measurements verified at two PV calibration laboratories [ISE (Germany), NREL (USA)]. *I–V* curves were obtained by applying an external bias to the cell and measuring the generated photocurrent with a Keithley model 2400 digital source meter. The voltage step and delay time of photocurrent were 10 mV and 40 ms, respectively. The photovoltaic measurements were taken by using a metal mask with an aperture area of 0.159 cm^2.

Electrical impedance spectroscopy

The electrochemical impedance measurements were performed with an Autolab PGstat30 potentiostat. A sinusoidal AC potential perturbation of 10 mV was overlaid over the applied DC bias potential. The frequency range applied for the AC perturbation was from 1 MHz to 0.1 Hz. The DC bias potential was applied in 50 mV steps.

The resulting impedance spectra were fitted in the simplest manner. The frequency range related to the recombination (so-called charge transfer) process was fitted with a simple RC element in series with a resistance. This latter resistance takes into account all other resistive elements in the device.

Results

We observed that, post-growth, the substrates are covered with vertically aligned nanowire arrays, whether they are synthesised without (Fig. 1(a) and (b)) or with (Fig. 1(c) and (d)) the additional additives. Higher resolution imaging highlights subtle differences in the films prepared with and without the additives. When no additives were used, individual nanowires resemble hexagonal prisms *i.e.* straight edged, six sided wires with D_{6h} symmetry (Fig. 1(a)). With the addition of the RE additives, individual wires have a hexagonal pyramid shape, with angled sides rising up to an apex at the tip of the nanowire *i.e.* C_{6v} symmetry (Fig. 1(c)).

XRD analysis, shown in Fig. 2, indicates that the unmodified and modified samples have similar crystal structures. Both samples can be indexed to the ZnO wurtzite crystal structure [JCPDF 75-0576] and have as their dominant peak the one centred at $2\theta = 34.4°$. This corresponds to the preferred orientation

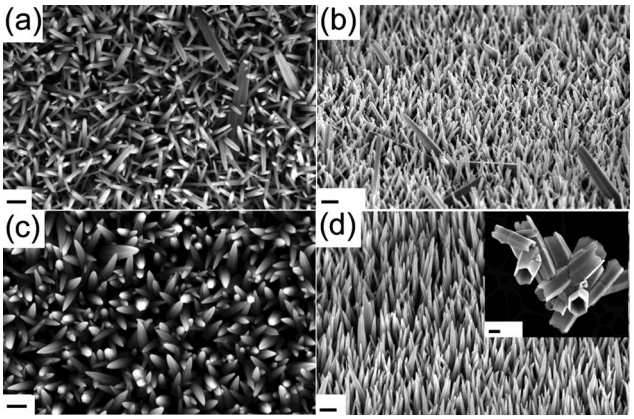

Fig. 1 SEM imaging of nanowire arrays formed under hydrothermal conditions. (a) Top view imaging of as-made ZnO nanowires; (b) 45° tilt imaging of the same ZnO nanowire array; (c) top view imaging of ZnO nanowires formed when 20 molar% yttrium nitrate is added to the growth solution (sample Y-ZnO-c); (d) 45° tilt imaging of the same Y-ZnO-c nanowire array, (*inset*) growth products formed in solution and filtered out post-growth. All scale bars correspond to 300 nm in length.

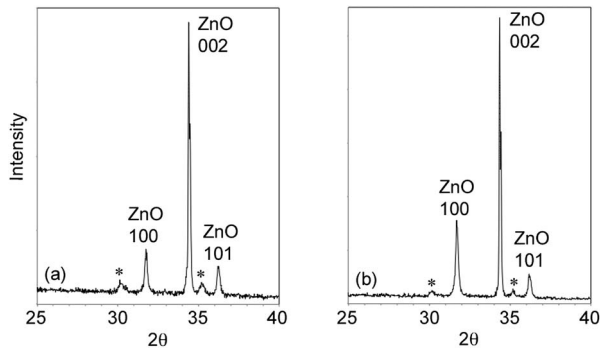

Fig. 2 XRD spectra of (a) ZnO and (b) Y-ZnO-c samples. *Substrate signals.

being in the (002) direction. No peak shifts or peak broadening is observed in the modified ZnO sample, implying that there has been no disruption or expansion of the lattice through dopant ion inclusion. The only noticeable difference is the decreased intensity of the (101) peak for the modified sample, explained through the observed crystal shape change. Therefore, structurally at least, the ZnO samples have similar crystallography.

The growth products obtained from the homogenous rather than the heterogeneous growth process (*i.e.* the precipitate in solution rather than the grown NW film) were filtered, washed and imaged under the SEM. Interestingly a "hollow" crystal morphology was observed for the Y-modified growth solution (Fig. 1(d), inset). Unmodified ZnO homogenous growth products tend to have a well-formed polyhedral structure. This "hollowed-rod" morphology is sometimes observed when growth solutions are within an intermediate supersaturation range and suggests a change in growth kinetics associated with the introduction of yttrium nitrate.[12] All samples have been tested within model DSSC devices, using the same dye and liquid electrolyte. Table 2 and Fig. 3 outline device performances for the unmodified and modified ZnO samples of around 1 μm length (at various mol% additives). For all additive

Table 2 Photovoltaic parameters of Y modified and unmodified ZnO samples at various concentrations with 1 μm length

Sample	V_{oc} (mV)	J_{sc} (mA cm^{-2})	FF	η
ZnO	497.2	2.06	0.29	0.3
Y-ZnO-a	678.7	2.73	0.48	0.91
Y-ZnO-b	668.6	2.26	0.59	0.91
Y-ZnO-c	711.1	2.2	0.62	0.98

concentrations, we see an extraordinarily large increase in the efficiency of the device. This is mainly driven by doubling of V_{oc} for the modified samples. Theoretically this could be a consequence of a number of factors, for example an increase in the amount of dye adsorbed on the ZnO film, an improved dye–ZnO binding interaction or a decrease in the recombination centres associated with the ZnO film. Since the thickness of the ZnO film is identical and the current density is almost the same, most increase in device performance must therefore be driven by the reduction in recombination.

Fig. 4(a) and (b) present the recombination resistance and capacitance measured by electrical impedance spectroscopy of the Y-modified ZnO DSSC and the unmodified ZnO DSSC and the corresponding dark current of those cells. It can be observed that in the case of the Y modified ZnO DSSC there is less recombination compared to the unmodified ZnO DSSC, which results in higher open circuit voltage and consequently to better device performance. The capacitance of the Y ZnO DSSC and the ZnO DSSC shown in Fig. 4(a) is further evidence that the increase in V_{oc} is due to the inhibition in the recombination and not as a result of a shift in the ZnO conduction band. There is a lack of shift in the ZnO bandgaps, confirmed with UV-Vis spectroscopy. A measurement of the absorption edge for unmodified and modified ZnO samples gives band gaps of 3.31 eV and 3.29 eV respectively, *i.e.* identical within the range of instrument errors.

Photoluminescence (PL), Raman and XPS were used to elucidate the reasons for why the addition of small quantities of rare earth additives into the growth solution could trigger such a large increase in efficiency. These techniques can be used to investigate crystal quality, defect quantity and dopant effect.[13] XPS depth profiles which were made by sputtering the sample for

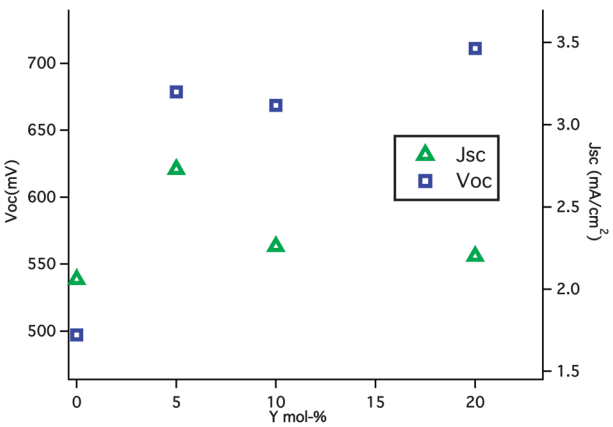

Fig. 3 Short circuit current density and open circuit voltage at different yttrium nitrate concentrations.

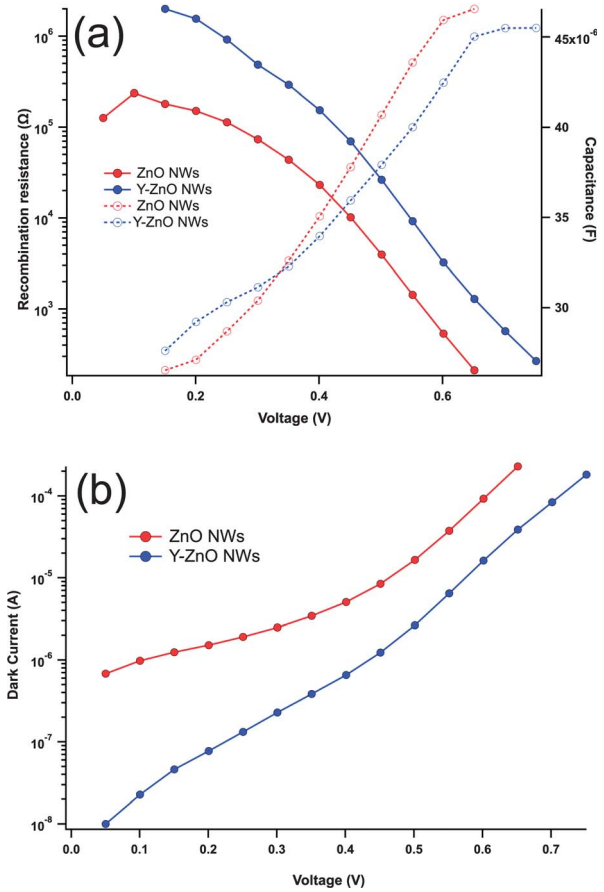

Fig. 4 (a) Recombination resistance (line) and capacitance (dashed line) measured by electrical impedance spectroscopy under dark of Y-ZnO-c (20%) modified ZnO and unmodified ZnO; (b) dark current measurements of the Y-ZnO-c (20%) modified ZnO and unmodified ZnO.

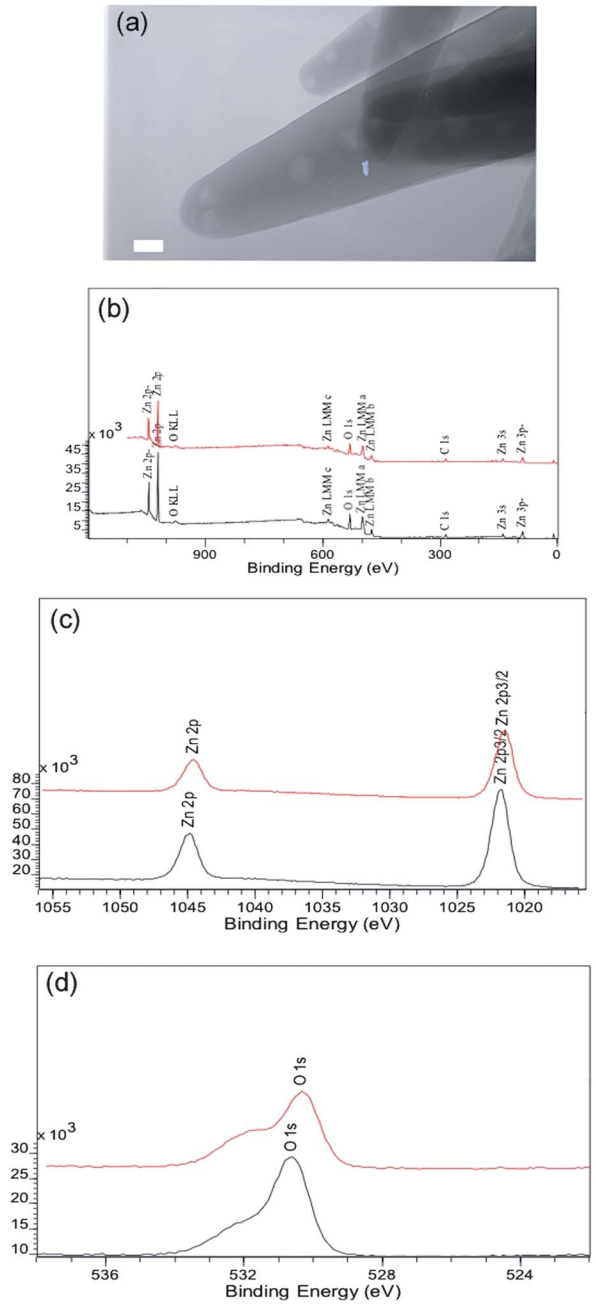

Fig. 5 HRTEM and XPS analysis of the Y-ZnO NW samples. (a) HRTEM showing the presence of cavities on the nanowire (scale bar = 20 nm); (b) XPS full scan spectra of ZnO (black) and Y-ZnO-c (red) samples; (c) detailed spectra of peaks associated with Zn 2p for ZnO (black) and Y-ZnO-c (red) samples; (d) detailed spectra of peaks associated with O 1s for ZnO (black) and Y-ZnO-c (red) samples.

5 min and EDX measurements of the film showed no evidence of Y-doping within the structure. Fig. 5 shows the XPS spectra of ZnO and Y-ZnO films. The binding energies have been calibrated to the carbon 1s reference peak (285 eV). The wide scan XPS spectra indicate peaks corresponding to the Zn2p1/2 (1044 eV), Zn2p3/2 (1021 eV), O 1s (530.4 and 531.7 eV) and C 1s (285 eV) energies. No Y peaks were observable. The peaks associated with O 1s (Fig. 5(c)) can be attributed to the two types of O present in the sample – the peak at 530.4 eV originates from the oxygen present in the crystal lattice;[14] the peak at 531.7 eV is from the oxygen chemisorbed on the surface of the crystal. Looking at the relative intensities of the peaks, the ratio of $Zn/O_{(cry)}$ for ZnO is 1.5 and for Y-ZnO is 1.4, *i.e.* a greater quantity of crystal lattice-associated oxygen in the Y-ZnO sample. This could be caused by fewer O-defects in the Y-ZnO sample than in the ZnO sample.[15] Additionally, there is a greater relative quantity of "chemisorbed" surface oxygen associated with the Y-ZnO sample. From the TEM images of the wires (Fig. 5(a)), this maybe associated with the presence of the observed cavities.

Fig. 6(a) shows the Raman spectroscopy of ZnO and Y-ZnO samples. Excitation was carried out with a 514.5 nm laser and laser power was kept low so as to not induce any heating or decomposition effects within the sample. The samples were grown on a Si wafer, and the peaks were normalised and calibrated to the strong Si peak at 520.5 nm. Only one characteristic peak associated with the ZnO lattice was observed at 438 cm^{-1}. This corresponds to the ZnO nonpolar optical phonons of the E_{2H} mode.[16] The intensity is greatest and the FWHM lowest for the Y-ZnO sample, suggesting a higher crystallinity for the Y-ZnO film.

Fig. 6(b) shows the room temperature photoluminescence spectra of different samples. The excitonic wavelength was

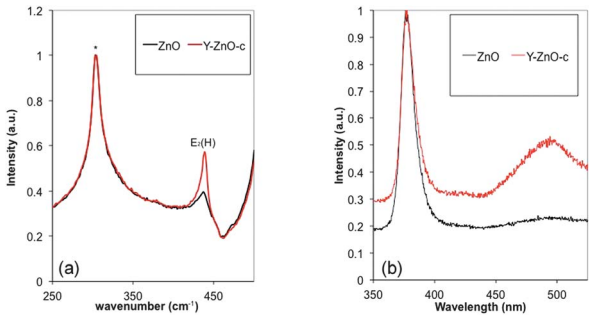

Fig. 6 (a) Raman spectroscopy of ZnO (black) and Y-ZnO-c (red) samples, taken with a 633 nm excitation laser. The peak (*) is associated with the Si substrate. (b) Room temperature photoluminescence spectra of ZnO (black) and Y-ZnO-c (red) samples, taken with an excitation wavelength of 325 nm.

325 nm and both spectra show two distinct regions: a sharper UV emission centred at ~375 nm and a broader emission between 430 and 550 nm. The UV emission is associated with recombination of the free excitons whilst the broader visible emission is associated with oxygen vacancies and zinc and oxygen interstitials.[17] Both samples show strong UV emission, confirming their high crystallinity. The Y-ZnO sample has a higher "defect" emission, centred in the blue region, which has been associated with a higher concentration of oxygen interstitials within the lattice.[18] It is worth noting that no 4f–4f inter-shell transitions from Y^{3+} ions can be observed,[19] again suggesting that no doping of the ZnO lattice has taken place.

We must therefore conclude that this decreasing recombination and increasing efficiency are not a consequence of any lattice doping of the rare earth species into the ZnO crystal. It is rather because of fundamental changes in the quality of the ZnO crystal formed. The increased basicity caused by the rare earth species may alter the growth rate of the nanostructures, slowing the growth kinetics and therefore improving the crystallinity of the as-made thin film.

It has previously been shown that further increases in DSSC efficiency can be obtained by increasing the thickness of the active layer to allow a greater amount of dye molecules to be adsorbed.[20] Growing ZnO NWs to any appreciable length is not trivial. Because of the propensity of the wire to undergo lateral expansion if kept unchecked during growth, structure directing agents such as polyethylene imine need to be introduced into the growth solution.[21] These agents preferentially bind to certain crystal facets of the ZnO, preventing growth in the lateral direction and promoting growth in the vertical "*c*" direction.[22] With this in mind, efforts were made to produce thicker active layers by the addition of PEI into the growth solution. When PEI was added to the growth solution containing Y-nitrate, no nanowires were seen to form. Instead, we obtained a non-crystalline closely packed layer. This is most likely due to side reactions taking place between yttrium nitrate and PEI, inhibiting the heterogeneous growth of the ZnO.

An alternative approach was tried and required separating out the two different growth regimes – the PEI growth solution to obtain longer NWs and the Y-nitrate growth solution to induce improvements in the crystal structure. Every 2 hours, the substrate was immersed in a fresh growth solution: either one containing the PEI-based precursors or one containing Y-based precursors. The final growth step was always for the Y-based precursors and the nanowires were always observed to have a pyramidal shape. In this way, wire lengths of up to 5 μm were obtained. As expected, the device performance improved as the wire length increased, as shown in Table 3.

From the results outlined in Table 3, the current density increases with the length of the wires due to the increase of the dye loading; however V_{oc} decreases as a result of more recombination due to the higher currents observed. Nevertheless, extremely promising device performances of 1.45% were achieved for nanowires with lengths of only 5 μm and by improving V_{oc} for these cells, we predicted that the efficiency should increase even further.

The use of core–shell structures has been shown to improve cell performances due to improved chemical binding stability of the sensitizers and removal of the surface defects in the underlying ZnO nanowires.[23] Previous work has shown that TiO_2 shells of 20 nm are extremely efficient in improving ZnO nanowire-based DSSCs constructed with C220 dye.[10] We therefore applied 20 nm TiO_2 shells to the Y-modified ZnO NWs in order to improve V_{oc}. Interestingly, only minor improvements in device performance were observed. Compared to the doubling of efficiency we previously reported for the shell on unmodified ZnO NW-based cells,[10] here it seems that the shell adds very little value to the overall NW structures.

Fig. 7(a) shows the *J*–*V* characteristic of the Y-ZnO coated with the 20 nm TiO_2 shell and Y-ZnO with the same wire length. When the Y-ZnO NWs are coated with the TiO_2 shell, V_{oc} increases by ≈175 mV and J_{sc} is slightly decreased from 4.1 to 3.8 mA cm^{-2}, which results in a small increase of the power conversion efficiency (η) to 1.52%. Since the current density is almost the same it can be assumed that the main reason for this increase in V_{oc} is due to recombination. To support this, Fig. 7(b) presents the impedance measurements, which were performed on those cells. As can be seen the recombination resistance is higher for the Y-ZnO/TiO_2 cell than that for the Y-ZnO cell, moreover the capacitance (Fig. 7(b)) indicates that there is no shift in the ZnO conduction band. As a result the higher V_{oc}, which was achieved for the TiO_2 coated Y-ZnO NWs, is due to less recombination.

Comparing our results with those available in the literature, both with and without TiO_2 shells, shows just how effective these ZnO NWs can be. For example, the work by Xu *et al.*[20] shows that wires need to be grown to approx. 17 μm in length before efficiencies of 1.5% can be obtained. Our wires show efficiencies of 1.45% when they are only 5 μm in length. Therefore our modified ZnO has achieved performances which may begin to compete with the traditional TiO_2-based DSSC devices. Increasing the length of the wires further may open up the

Table 3 Different lengths of Y-modified ZnO NWs grown by the separation of the two growth regimes

NWs length (μm)	V_{oc} (mV)	J_{sc} (mA cm^{-2})	FF	η
1	711.1	2.2	0.62	0.98
3	676.3	3.15	0.54	1.17
4	655.1	3.65	0.54	1.3
5	614.6	4.1	0.58	1.45

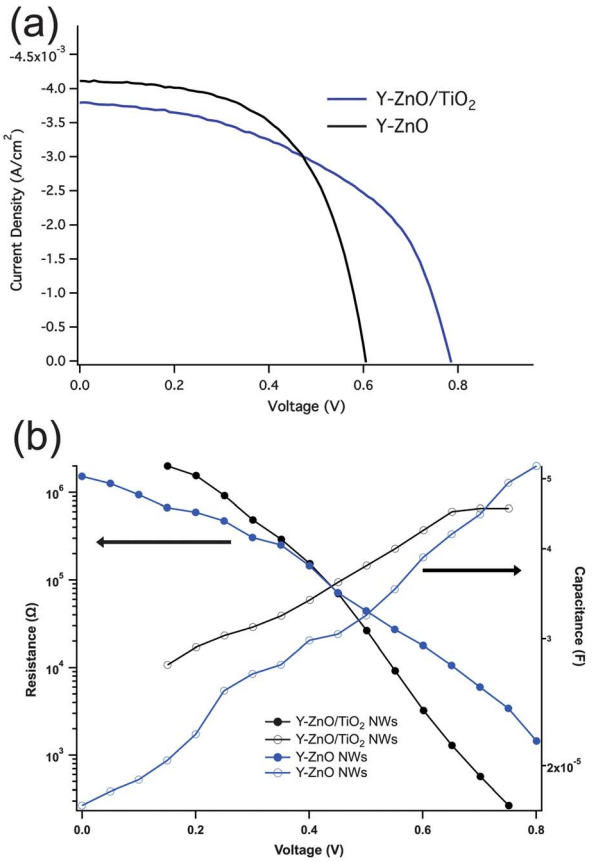

Fig. 7 (a) *J–V* characteristic of Y-ZnO/TiO_2 and Y-ZnO cells under 1 sun illumination; (b) recombination resistance and capacitance of both cell conditions made by impedance spectroscopy under dark.

possibility to obtain ZnO with superior performance to TiO_2 nanoparticle DSSCs.

Conclusions

We have demonstrated a new ZnO active layer which shows superior performance when used within dye sensitised solar cells. Our characterisation indicates that this ZnO has a much higher crystalline quality than the ZnO produced using conventional methods. The photovoltaic performance and impedance measurements indicate that the increased device efficiencies are driven by blocking recombination sites on the ZnO surface. This ensures that good device performance is obtained, even without the need for subsequent surface treatments. We have developed a new method to produce longer modified nanowires, up to 5 μm, with a device efficiency of 1.45% rising to 1.5% when a thin TiO_2 shell is applied to the active layer.

Acknowledgements

This research was funded by the European Community's Seventh Framework Programme (FP7/2007-2013) under grant agreement no. 227057, project "INNOVASOL". L.E. acknowledges the Marie Curie Actions—Intra-European Fellowships (FP7-50 PEOPLE-2009-IEF) under grant agreement no. 252228, project "Excitonic Solar Cell". The authors thank Dr Suman-Lata Sahonta for HRTEM characterization.

Notes and references

1 L. M. Peter, *J. Phys. Chem. Lett.*, 2011, **2**, 1861–1867.
2 B. O'Regan and M. Graetzel, *Nature*, 1991, **353**, 737–740.
3 S. Yodyingyong, Q. Zhang, K. Park, C. S. Dandeneau, X. Zhou, D. Triampo and G. Cao, *Appl. Phys. Lett.*, 2010, **96**, 073115.
4 M. Saito and S. Fujihara, *Energy Environ. Sci.*, 2008, **1**, 280–283.
5 N. Sakai, N. Kawashima and T. N. Murakami, *Chem. Lett.*, 2011, **40**, 162–164.
6 J. S. Bendall, G. Visimberga, M. Szachowicz, N. O. V. Plank, S. Romanov, C. M. Sotomayor-Torres and M. E. Welland, *J. Mater. Chem.*, 2008, **18**(43), 5259–5266.
7 S. Cho, S.-H. Jung, J.-W. Jang, E. Oh and K.-H. Lee, *Cryst. Growth Des.*, 2008, **12**, 4553–4558.
8 I. Gonzalez-Valls and M. Lira-Cantu, *Energy Environ. Sci.*, 2009, **2**(1), 19–34.
9 N. O. V. Plank, H. J. Snaith, C. Ducati, J. S. Bendall, L. Schmidt-Mende and M. E. Welland, *Nanotechnology*, 2008, **19**, 46.
10 J. S. Bendall, L. Etgar, S. C. Tan, N. Cai, P. Wang, S. M. Zakeeruddin, M. Greatzelb and M. E. Welland, *Energy Environ. Sci.*, 2011, **4**, 2903–2908.
11 N. Cai, S.-J. Moon, L. Cevey-Ha, T. Moehl, R. Humphry-Baker, P. Wang, S. M. Zakeeruddin and M. Grätzel, *Nano Lett.*, 2011, **11**(4), 1452–1456.
12 K. Govender, D. S. Boyle, P. B. Kenway and P. O'Brien, *J. Mater. Chem.*, 2004, **14**, 2575–2591.
13 A. Djelloul, M. S. Aida and J. Bougdira, *J. Lumin.*, 2010, **130**(11), 2113–2117.
14 J. Yang, X. Li, J. Lang, L. Yang, M. Gao, X. Liu, M. Wei, Y. Liu and R. Wang, *J. Alloys Compd.*, 2011, **509**, 10025–10031.
15 F. Hai-Bo, Y. Shao-Yan, Z. Pan-Feng, W. Hong-Yuan, L. Xiang-Lin, J. Chun-Mei, Z. Qin-Sheng, C. Yong-Hai and W. Zhan-Guo, *Chin. Phys. Lett.*, 2007, **24**, 2108.
16 C. X. Xu, X. W. Sun, X. H. Zhang, L. Ke and S. J. Chua, *Nanotechnology*, 2004, **15**, 856–861.
17 P.-T. Hsieh, Y.-C. Chen, K.-S. Kao and C.-M. Wang, *Appl. Phys. A: Mater. Sci. Process.*, 2008, **90**, 317–321.
18 R. Chen, Y. Q. Shen, F. Xiao, B. Liu, G. G. Gurzadyan, Z. L. Dong, X. W. Sun and H. D. Sun, *J. Phys. Chem. C*, 2010, **114**, 18081–18084.
19 X. Zeng, J. Yuan and L. Zhang, *J. Phys. Chem. C*, 2008, **112**, 3503–3508.
20 C. Xu, P. Shin, L. Cao and D. Gao, *J. Phys. Chem. C*, 2010, **114**, 125–129.
21 M. Law, L. Greene, J. C. Johnson, R. Saykally and P. Yang, *Nat. Mater.*, 2005, **4**, 455.
22 L. E. Greene, B. D. Yuhas, M. Law, D. Zitoun and P. Yang, *Inorg. Chem.*, 2006, **45**, 7535.
23 M. Law, L. E. Greene, A. Radenovic, T. Kuykendall, J. Liphardt and P. Yang, *J. Phys. Chem. B*, 2006, **110**(45), 22652–22663.

